

Accretion dynamics and disk evolution in NGC 2264: a study based on the Corot[★] photometric observations

S.H.P. Alencar¹, P.S. Teixeira², M.M. Guimarães^{1,3}, P.T. McGinnis¹, J.F. Gameiro⁴, J. Bouvier⁵, S. Aigrain^{6,7}, E. Flaccomio⁸ and F. Favata⁹

¹ Departamento de Física – ICEx – UFMG, Av. Antônio Carlos, 6627, 30270-901, Belo Horizonte, MG, Brazil

² ESO, Karl-Schwarzschild-Strasse 2, D-85748 Garching bei München, Germany

³ UFSJ – Campus Alto Paraopeba – Rodovia MG 443, KM 7, 36420-000, Ouro Branco, MG, Brazil

⁴ Centro de Astrofísica da Universidade do Porto, Rua das Estrelas, 4150 Porto, Portugal

⁵ Laboratoire d'Astrophysique, Observatoire de Grenoble, BP 53, F-38041 Grenoble Cédex 9, France

⁶ School of Physics, University of Exeter, Exeter, EX4 4QL, UK

⁷ Astrophysics, University of Oxford, Denys Wilkinson Building, Oxford, OX4 1DQ, UK

⁸ INAF - Osservatorio Astronomico di Palermo, Piazza del Parlamento 1, 90134 Palermo, Italy

⁹ European Space Agency, 8-10 rue Mario Nikis, 75015 Paris, France

Received ; accepted

ABSTRACT

Context. The young cluster NGC 2264 was observed with the Corot satellite for 23 days uninterruptedly in March 2008 with unprecedented photometric accuracy. We present here the first results of the analysis of the accreting population that belongs to the cluster and was observed by Corot.

Aims. We intended to look for possible light curve variability of the same nature as that observed in the classical T Tauri star AA Tau, which was attributed to a magnetically controlled inner disk warp. The inner warp dynamics is directly associated with the interaction between the stellar magnetic field and the inner disk region.

Methods. We analysed the Corot light curves of 83 previously known classical T Tauri stars that belong to NGC 2264 and classified them according to their morphology. We also studied the Corot light curve morphology as a function of a *Spitzer*-based classification of the star-disk systems.

Results. The classification derived on the basis of the Corot light curve morphology agrees very well with the *Spitzer* IRAC-based classification of the systems. The percentage of AA Tau-like light curves decreases as the inner disk dissipates, from $40\% \pm 10\%$ in systems with thick inner disks to $36\% \pm 16\%$ in systems with anemic disks and none in naked photosphere systems. Indeed, $91\% \pm 29\%$ of the CTTS with naked photospheres exhibit pure spot-like variability, while only $18\% \pm 7\%$ of the thick disk systems do so, presumably those seen at low inclination and thus free of variable obscuration.

Conclusions. AA Tau-like curves are found to be fairly common, with a frequency of at least ~ 30 to 40% in young stars with inner dusty disks. The temporal evolution of the light curves indicates that the structure of the inner disk warp, located close to the corotation radius and responsible for the obscuration episodes, varies over a timescale of a few (~ 1 - 3) rotational periods. This probably reflects the highly dynamical nature of the star-disk magnetospheric interaction.

Key words. Stars: pre-main sequence – Techniques: photometry – Accretion, accretion disks

1. Introduction

T Tauri stars are young, optically visible, low-mass stars still contracting toward the main sequence. They have strong magnetic fields (~ 2 kG) and are X-ray emitters. The so-called weak line T Tauri stars (WTTs) do not exhibit evidence of disk accretion, while the classical T Tauri stars (CTTSs) do. CTTSs present broad emission lines and sometimes also forbidden emission lines. They are spectroscopically and photometrically variable, and show ultraviolet (UV), optical and infrared (IR) excess with respect to the photospheric flux.

Magnetospheric accretion models are the current consensus to explain the main observed characteristics of CTTSs

(Shu et al., 1994; Hartmann et al., 1994; Muzerolle et al., 2001; Kurosawa et al., 2006). In these models, the stellar magnetosphere is strong enough to disrupt the circumstellar disk at a few stellar radii. Material in the inner disk, ionized by stellar radiation, falls towards the star following magnetic field lines and hits the stellar photosphere at near free-fall velocities, creating hot spots on the stellar surface. Part of the ionized material in the inner disk region is ejected in a magnetically controlled wind. In this scenario, the broad permitted emission lines are formed partly in the accretion funnel and the hot spot emits a continuum flux that is responsible for the UV and optical excess that veils the photospheric lines. The IR excess comes from reprocessing by the dust in the disk of the stellar and accretion radiation and, at least for high accretion rate systems, viscous heating may also contribute to it. When observed, forbidden emission lines are thought to be formed in the low density wind.

In the last decade, numerical simulations of accreting young stars have predicted a very dynamical star-disk interaction,

Send offprint requests to: silvia@fisica.ufmg.br

★ The CoRoT space mission was developed and is operated by the French space agency CNES, with participation of ESA's RSSD and Science Programmes, Austria, Belgium, Brazil, Germany, and Spain

mediated by the stellar magnetic field (Goodson et al., 1999; Matt et al., 2002; Romanova et al., 2009; Zanni, 2009). Many magneto-hydrodynamical (MHD) model predictions derive from the idea that the stellar magnetic field interacts with the inner disk region near the co-rotation radius but not only at the co-rotation point. Consequently, due to differential rotation between the star and the inner disk region, the magnetic field lines become distorted after a few rotational periods and eventually reconnect, restoring the initial field configuration. This process goes on as the star rotates. The time scale for the reconnection events depends on the diffusivity of the stellar magnetic field lines in the inner disk region, which is a very poorly constrained parameter.

AA Tau is one of a few CTTSs studied with enough detail to test the MHD model dynamical predictions. The star was observed photometrically for a month during three different campaigns, two of which included high-resolution simultaneous spectroscopy (Bouvier et al., 1995, 2003, 2007). AA Tau shows a light curve (LC) with a flat maximum interrupted by deep quasi-periodical minima that vary in depth and width from one rotational cycle to the other. The minima occur with little color change and are thought to be due to obscuration of the stellar photosphere by circumstellar disk material present in an inner disk warp. The warp is due to the interaction of the stellar magnetic field, inclined with respect to the rotation axis, and the inner disk region. The spectroscopic results showed that the magnetic field lines inflate in the course of a few rotational cycles, as measured by the radial velocity of the red and blue absorption components of the $H\alpha$ line. Moreover, when the field lines are the most inflated, accretion to the star is suppressed, with no apparent veiling, and low emission-line equivalent widths, which again corroborates the MHD model predictions. After reconnection, accretion starts all over again. The last two AA Tau observational campaigns were separated by 5 years and the field line inflation discovered in the second campaign was still present with the same characteristics in the third one.

Although the AA Tau observations gave strong support to the MHD results, it was still unclear whether this behaviour was common among CTTSs. In order to test this, one needs good photometric measurements of a large number of CTTSs, covering several rotational cycles. In Taurus the typical rotational period of a CTTS is around 8 days, so that stars need to be monitored for at least a month continuously. This is not an easy task from the ground, due to telescope time allocation and weather conditions. The Corot satellite additional program to observe the young stellar cluster NGC 2264 has allowed us to perform such study on a large sample of CTTSs.

NGC 2264 is a well studied young stellar cluster with an age of ≈ 3 Myr located at a distance of about 760 pc (see Dahm, 2008, for a recent review on the cluster). We matched the various available datasets on the cluster from the literature based on spatial coincidence using a $2''$ tolerance. In a small number of cases, double identifications (i.e. more than one object within $2''$) were transformed into single ones, specifically in cases in which one of the two objects had a small offset and the other a large one. Due to the many studies on the cluster, going from UV to X-rays, it was possible to establish reasonable criteria for cluster membership. We considered as likely members of NGC 2264 stars selected according to one or more of the following criteria: i) photometric $H\alpha$ and variability with the data of Lamm et al. (2004) and following their criteria, ii) X-ray detection (Ramírez et al., 2004; Flaccomio et al., 2006) and location on the cluster sequence in the $(I, R - I)$ diagram if R and I magnitudes are available, iii) spectroscopic $H\alpha$ equivalent width greater than 10 \AA

and iv) $H\alpha$ emission line width at 10% intensity greater than 270 km s^{-1} , as proposed by White & Basri (2003) to identify accreting T Tauri stars, and measured by Fűrész et al. (2006) for many cluster members.

The mean rotational period of CTTSs in NGC 2264 is around 3 to 4 days (see Sect. 4). Corot observed the cluster for 23 days uninterruptedly, covering several rotational cycles for most of the stars, thus allowing the identification of AA Tau-like candidates and the determination of precise rotational periods for cluster members. The complete rotation analysis will be discussed separately in another paper (Affer et al. in preparation).

2. Observations

Corot observed NGC 2264 from the 7th to the 30th of March 2008. The whole cluster fitted in one of the two CCDs normally used for the exo-planet observations, and stars were observed down to $R \approx 18$. We used the light curves delivered by the Corot pipeline after nominal corrections (Samadi et al., 2007). We further corrected the pipeline light curves removing outliers, mainly due to the South Atlantic Anomaly crossings, by applying a sigma clipping filter, taking care not to remove flaring events. The data was also corrected for the effects due to the entrance and exit into Earth eclipses. We did not make use of the color information provided by Corot for the brightest stars, and based our analysis on the broadband, “white light” light curves. All the light curves presented here were rebinned to 512 s and correspond to the integrated flux in the Corot mask. The flux RMS over 512 s achieved is of the order of 0.0005 for a $R = 12$ star and 0.004 for a $R = 16$ star, yielding the most detailed light curves of young accreting systems up to now, as shown in Figure 1. A complete catalog of the observations will be published in a subsequent paper (Favata et al. in preparation).

3. Results

3.1. Classical T Tauri sample selection

After selecting the cluster members as described in Sect. 1, we classified as CTTSs stars that presented either $H\alpha$ equivalent width greater than 10 \AA , $U - V$ excess less than a threshold calculated below, or $H\alpha$ width at 10% intensity greater than 270 km s^{-1} . Some stars presented more than one of the above characteristics. White & Basri (2003) showed that the accretion criterion based on $H\alpha$ equivalent width is spectral-type dependent, the threshold being smaller than 10 \AA for spectral types earlier than K7 and greater than 10 \AA for spectral types later than M2.5. Whenever spectral type information was available, we followed the accretion criteria proposed by White & Basri (2003), instead of using the standard 10 \AA value. Rebull et al. (2002) proposed that stars in NGC 2264 with $U - V$ excess less than -0.5 could be classified as disk candidates. This threshold value was based on a study of the Orion star forming region (Rebull et al., 2000). However, the $U - V$ excess is also expected to be spectral-type dependent, stars with later spectral types presenting higher $U - V$ excess compared to earlier ones, for the same mass accretion rate, due to the higher contrast between the hot spot and the stellar photosphere in later spectral types. Therefore we looked for all the stars of our sample that were selected as CTTS based on $U - V$ excess and another criterion ($H\alpha$ equivalent width or

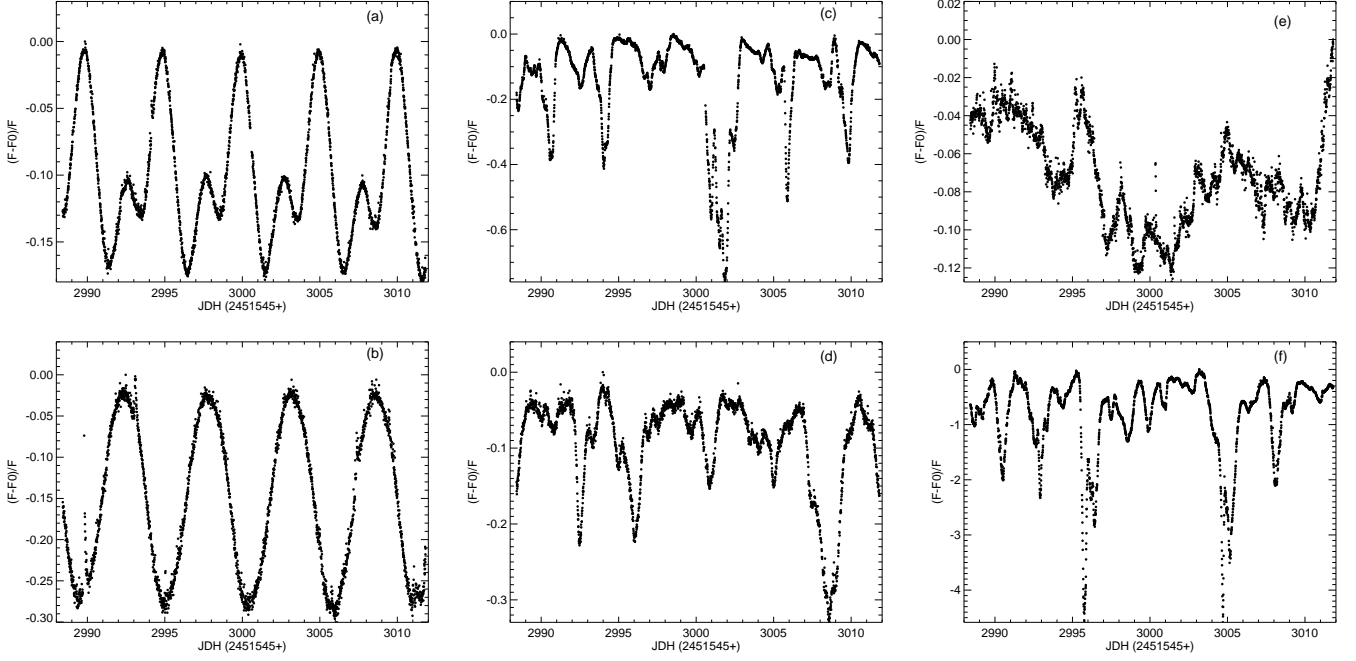


Fig. 1. A sample of 6 CTTS light curves from the COROT observation of NGC 2264. F_0 corresponds to the maximum flux value of each LC. Light curves *a* and *b* have been classified as spot-like, *c* and *d* as AA Tau-like and *e* and *f* as irregular.

$H\alpha$ width at 10% intensity). We separated them in two spectral type ranges (K0-K6 with 14 stars and K7-M3 with 10 stars) and computed the mean $U - V$ excesses in each dataset. The K0-K6 CTTSs present $U - V$ excess of -1.06 ± 0.48 mag and the K7-M3 CTTSs present $U - V$ excess of -1.69 ± 0.57 mag. Using the one sigma upper boundary in each spectral type range as a threshold to separate CTTSs from WTTS (-0.58 for K0-K6 and -1.12 for K7-M3), we select 7 stars as CTTSs based only on $U - V$ excess. While the value of -0.5 mag proposed by Rebull et al. (2002) seems to be adequate for stars in the K0-K6 spectral range, it is apparently too high to select K7-M3 CTTSs in NGC 2264.

We found 83 CTTSs among the 301 observed cluster members and present in Table 1 the data used to make the CTTS classification. The $H\alpha$ equivalent width was taken from Rebull et al. (2002) and Dahm & Simon (2005) except for six stars (CID 223957455, 223959618, 223964667, 223968688, 223991832, 223994721) for which we measured the $H\alpha$ equivalent width ourselves, using the high resolution hectoéchelle spectra kindly provided by Gabor Fűrész. The $U - V$ excess data was obtained from Rebull et al. (2002) and Fallscheer & Herbst (2006) (the data table was kindly provided by Cassandra Fallscheer) and the $H\alpha$ width at 10% intensity comes from Fűrész et al. (2006).

Some CTTSs that were selected based on their $U - V$ excess have $H\alpha$ values that are below 10 \AA and would therefore not be selected as CTTS based only on $H\alpha$ equivalent width. However, their $U - V$ excess is lower than our established threshold values and in the same range as many other systems that present either $H\alpha$ equivalent width greater than 10 \AA or $H\alpha$ width at 10% larger than 270 km s^{-1} . We have to be aware that both $H\alpha$ equivalent width and $U - V$ excess are strongly variable in these stars and were not measured simultaneously. So it seems reasonable to use both criteria to select possible CTTSs.

3.2. Morphological light curve classification

We looked for periodical variations in the LCs of the observed CTTSs, using the Scargle periodogram as modified by Horne & Baliunas (1986), and found that 51 out of 83 CTTSs presented periodical variability. Periodic LCs were divided in two groups: group PI, containing sinusoidal-like LCs with stable shape from cycle to cycle, and group PII, flat-topped LCs with a clear maximum interrupted by minima that can vary in width and depth from cycle to cycle. The variations in group PI are associated with long-lived spots with lifetime of at least of weeks, while group PII is associated with AA Tau-like systems, where most of the variability is due to obscuration by circumstellar disk material. The non-periodical LCs (group NP) can be due to obscuration by non-uniformly distributed circumstellar material or to non-steady accretion or both.

A total of 83 CTTSs that belong to NGC 2264 were observed by Corot, 28 of which were classified as spot-like (group PI), 23 as AA Tau-like (group PII) and 32 as irregular (group NP). A sample of light curves of each type is shown in Fig. 1. In Figure 2 we present the periodical LCs of Fig. 1 folded in phase with the periods determined with the Scargle periodogram as modified by Horne & Baliunas (1986). We can notice the stability of the spot-like LCs (Fig. 1 and Fig. 2 *a* and *b*) in the timescale of the observations, which makes them, in general, easily distinguishable from the AA Tau-like ones (Fig. 1 and Fig. 2 *c* and *d*). Among the irregular LCs, some look more like due to variable accretion events (variable hot spots, Fig. 1 *e*) and others to obscuration by non-uniform circumstellar material (Fig. 1 *f*), but it is hard to decide which process is the dominant one based only on the Corot light curves without any color information. Therefore we did not make any attempt to further classify the irregular systems.

We measured the variability amplitude of a LC as $((\text{Flux}_{\text{max}} - \text{Flux}_{\text{min}}) / \text{Flux}_{\text{median}}) \times 100$. In our sample, the observed CTTS variability amplitudes range from 3% to 137%, excluding flaring events. The variability amplitude of spot-like LCs is gener-

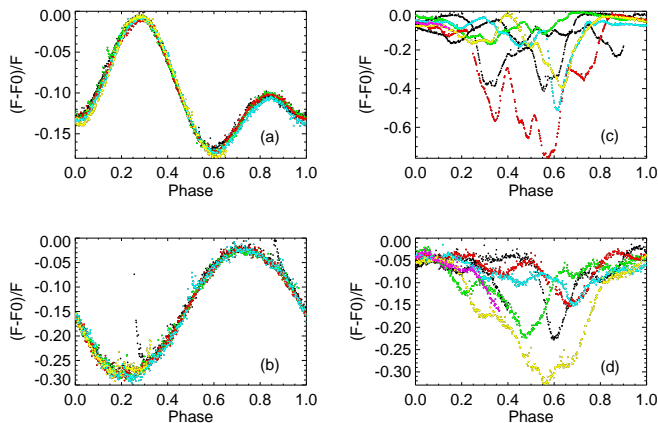


Fig. 2. The four periodic LCs from Fig. 1 folded in phase. Different colors correspond to different cycles.

ally around 10% to 15% and most of the stars that present more than 20% of variability amplitude have LCs that are classified as due to obscuration by circumstellar material (AA Tau-like). The AA Tau system variability amplitude, measured from data in the literature, is 76% and 8 out of 83 stars observed by Corot have a higher variability amplitude than AA Tau. This shows that, although AA Tau presents a high variability amplitude, probably due to its high inclination with respect to our line of sight ($\sim 75^\circ$ Bouvier et al., 2003), it is not exceptional among CTTS systems.

From the results in this Section, it becomes clear that the AA Tau photometric behavior is not an exception, but a rather common occurrence among young stellar systems, representing $28\% \pm 6\%$ of the CTTS systems in NGC 2264 observed with Corot. The percentage of AA Tau-like systems among the observed CTTSs seems reasonable, given that only some geometric configurations (i.e. high inclination) would produce occultation of the stellar photosphere, and the chances for occultation events will also depend on the disk warp's location and scale-height. This result is however higher than the value of 10% to 15% calculated by Bertout (2000) using flared disk models for the probability of observing partial occultation events in CTTS systems. However, the disk models by Bertout (2000) did not include an inner disk warp, and consequently underestimate the probability of obscuration. Assuming a random distribution of axial inclinations, the fraction of AA Tau-like LCs in our sample ($\geq 28\%$) suggests $h/r \sim 0.3$ for inner disk warps, where h and r are the inner warp height and distance to the central star. This is larger than the standard value used in α -disk models, where $h/r \sim 0.05 - 0.1$ (Bertout et al., 1988; Duchêne et al., 2010).

3.3. Merging Corot and Spitzer data

Spitzer IRAC data were also available for the cluster (Teixeira, 2008), with a total of 68 CTTSs present in both *Spitzer* and Corot observations. IRAC is useful to identify near-infrared excess emission that arises from warm dusty circumstellar material. We used the α_{IRAC} index, which represents the slope of the spectral energy distribution between $3.6 \mu\text{m}$ and $8 \mu\text{m}$, to classify the inner disk structure of the observed systems, following the criteria proposed by Lada et al. (2006). Stars with $\alpha_{\text{IRAC}} < -2.56$ are classified as naked photospheres (i.e., these systems are devoid of dust within a few AU), stars with $-2.56 < \alpha_{\text{IRAC}} < -1.80$ have anemic disks (optically thin inner disks), stars with $-1.80 < \alpha_{\text{IRAC}} < -0.5$ have optically thick inner disks (referred

to as thick disks henceforth), those with $-0.5 < \alpha_{\text{IRAC}} < 0.5$ are flat spectra sources and the ones with $\alpha_{\text{IRAC}} > 0.5$ are Class I objects.

We combined both datasets in order to see if the light curve morphology was related to the evolution of the inner disk structure. The result, presented in Figure 3, shows that the agreement between the two classification approaches of CTTS (based on the Corot light curves and on the *Spitzer* photometry) is excellent. None of the systems with naked photospheres exhibit AA Tau-like LCs and 10/11 ($91\% \pm 29\%$) of them show pure spot-like variability. The percentage of AA Tau-like LCs, which are due to obscuration by circumstellar disk material, thus increases from 0% for the evolved inner disk systems (naked photospheres) to $36\% \pm 16\%$ for the anemic disk systems and $40\% \pm 10\%$ for the thick disk systems. Because some of the non-periodic LCs may also be partly caused by circumstellar obscuration (see a possible example in Fig. 1f), the fractional estimates of obscuration LCs are lower limits for systems with anemic and thick disks.

Spot-like systems represent $91\% \pm 29\%$ of the naked photospheres, $28\% \pm 14\%$ of the anemic disks and $18\% \pm 7\%$ of thick disk systems. They are observed in systems where there is no obscuring material in our line of sight towards the star. This could be due to inner disk clearing, corresponding to spot-like LCs which represent naked photosphere systems and some anemic disks, shown in Fig. 3. Spot-like LCs could also come from low inclination systems. In this case, there could be inner disk material, but it would not obscure the star. This probably corresponds to some anemic disk systems and to all thick disk systems that show spot-like LCs.

The non-periodical LCs represent $9\% \pm 9\%$ of the naked photospheres, $36\% \pm 16\%$ of the anemic disks and $42\% \pm 10\%$ of the thick disk systems. The irregular LCs among naked photosphere systems can be due to non-steady accretion, which will produce short-lived and variable hot spots. Some irregular systems among anemic disks and thick disks are also likely due to a combination of non-steady accretion and low inclination, as apparently observed in TW Hya (Rucinski et al., 2008). It may however not be straightforward to assign non-periodical LCs to non-steady accretion, as recently shown by Kulkarni & Romanova (2009). They computed MHD models of the interaction between a magnetized star and its circumstellar disk with non-steady accretion and showed that, at large misalignment angles ($\theta > 25^\circ$) between the stellar rotation and magnetic axis, hotspots are approximately fixed on the star's surface, even during strongly unstable accretion, and consequently the LCs always show the stellar rotation period. Assuming that the circumstellar environment of a CTTS may be complex, random accretion events due to circumstellar blobs, which fall towards the star, could also temporarily occult the star and explain some of the observed non-periodical systems, as proposed by DeWarf et al. (2003) to explain the irregular photometric variability of the CTTS SU Aur. Another situation that could produce irregular LCs is a flared disk seen at high inclination. We could then expect to see partial obscuration by circumstellar disk material from the disk outer layers. Bertout (2000) calculated the partial obscuration probability by a flared disk and showed that, for a typical CTTS, it would be of the order of 10% to 15%. In this case, assuming Keplerian disk rotation and a typical CTTS disk with an outer radius of 100 AU, we would unfortunately not be able to measure short scale variability, as observed with Corot, due to material located in most disk radii because of the limited duration of our observations.

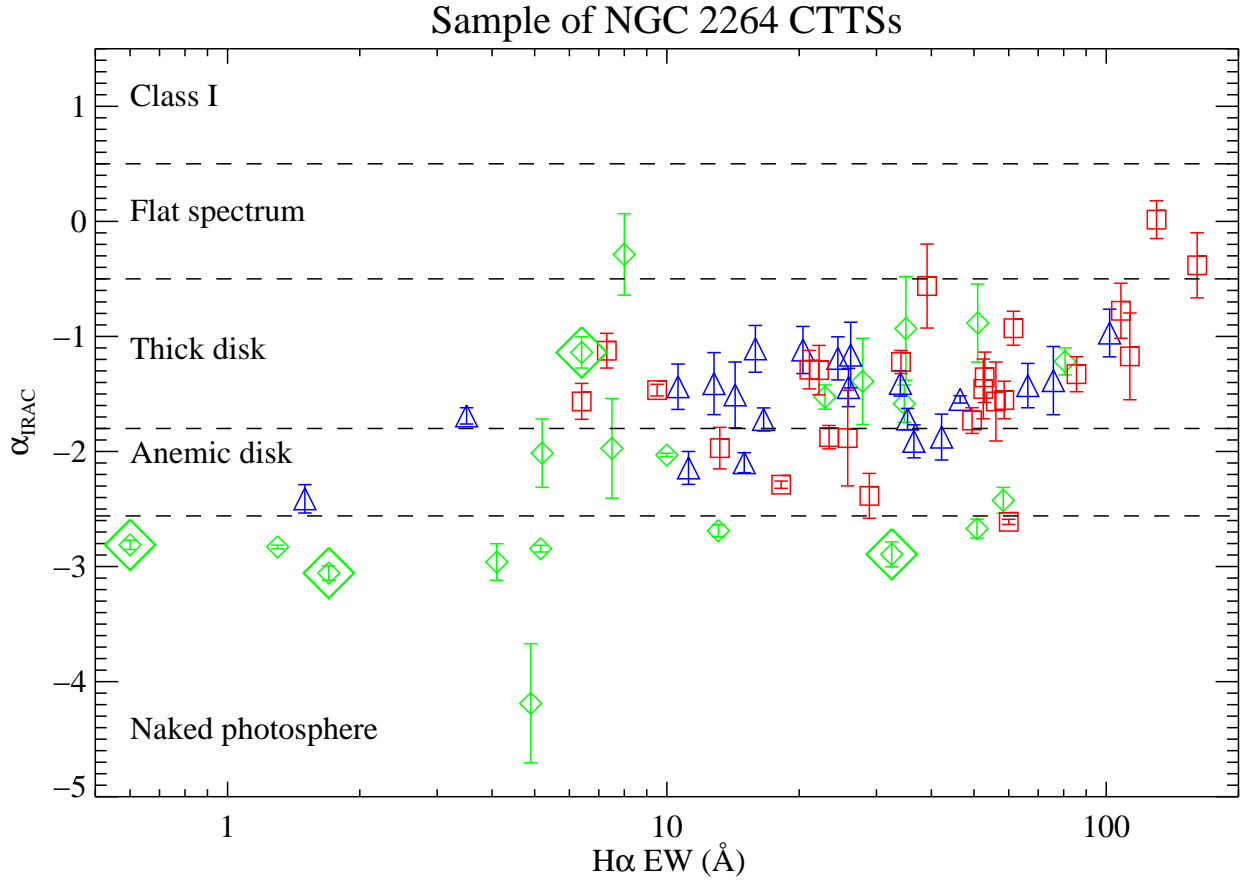


Fig. 3. NGC 2264 classical T Tauri stars observed with *Corot* and *Spitzer*. Diamonds correspond to spot-like LCs, triangles to AA Tau-like LCs and squares to non-periodical LCs. The four stars with large overplotted diamonds are fast rotators ($p < 2$ days). One fast rotator was not included in this figure (CID 500007354, $p = 1.17$ days), because of the huge uncertainty (2.89) on its α_{IRAC} index. It is nevertheless included in Table 1 and in our LC analysis.

4. Discussion

We calculated periods for all CTTs that presented periodic variations (51 out of 83 CTTs), using the Scargle periodogram as modified by Horne & Baliunas (1986). We present in Fig. 4 the period distribution of the spot-like (black histogram) and AA Tau-like (red histogram) systems. A complete discussion on period distribution in NGC 2264 is presented in another paper (Affer et al. in preparation).

The major difference between the period distributions of spot-like and AA Tau-like systems is that fast rotators ($p < 2$ days) are only found with spot-like LCs. Among the seven fast rotating CTTs, five also have *Spitzer* IRAC measurements. Four of them are classified as naked photosphere systems and another is a thick disk system. The thick disk system (CID 223980447, $\alpha_{\text{IRAC}} = -1.14 \pm 0.13$, $p = 1.67$ days) is a K6 star (Dahm & Simon, 2005) and has high-resolution hectochelle spectra (Fűrész et al., 2006) that Gabor Fűrész kindly made available to us. We measured $v \sin i = 30 \text{ km s}^{-1}$, using the SYNTH3 code provided by Dr. Oleg Kochukhov (Kochukhov, 2007), together with MARCS atmospheres (Gustafsson et al., 2008) and atomic lines from VALD (Kupka et al., 2000, 1999). Assuming $R_* = 2 R_{\odot}$, we obtain $i = 29.4^{\circ}$. This low inclination can explain the presence of circumstellar material with no obscuration in the LC. Except for this system, most fast rotators are found among systems that have cleared out their inner disk regions, which could be an indication that as the star-disk coupling

decreases, stars tend to spin-up, as also found by Rebull et al. (2006) and Cieza & Baliber (2007) in Orion and NGC 2264. This is not a straightforward conclusion, however, from our data, since the number of fast rotators is small and on the other hand some naked photosphere and anemic disk systems are actually found to rotate slowly, with periods up to 10 to 15 days.

The periods measured in the AA Tau-like LCs fall in the range of periods obtained from spot-like LCs. The periods measured from the spot-like LCs correspond to stellar rotational periods, since spots are located at the stellar photosphere. This indicates that AA Tau-like periods are within the range of stellar rotational periods of CTTs in NGC 2264 and therefore the material that obscures the star must be located close to the corotation radius. Since the inner warp is by definition located close or at the dust disk truncation radius, this implies that the dust truncation radius is near the corotation radius in the systems we classified as AA Tau-like. Carr (2007) showed that the inner gas radius is on average slightly smaller than the corotation radius, while the inner dust radius falls at or outside the corotation radius. This is quite consistent with the *Corot* results.

Since the inner disk warp is located near the corotation radius, the variations observed from cycle to cycle in width and depth of the photometric minima should be related to the dynamical star-disk interaction in the inner disk region, that is thought to be responsible for the accumulation of material near the disk truncation region, forming inner disk warps. Like AA

Tau, the star-disk interaction is seen to be very dynamic on a rotational timescale, as predicted by MHD models of young magnetized star-disk systems (Goodson et al., 1999; Matt et al., 2002; Romanova et al., 2009; Zanni, 2009). In our observations some systems are more regular and stable than others, but it is quite common to see systems that present photometric minima that vary substantially from cycle to cycle, still keeping their overall periodic nature (see Figs. 1, 2 *c* and *d*).

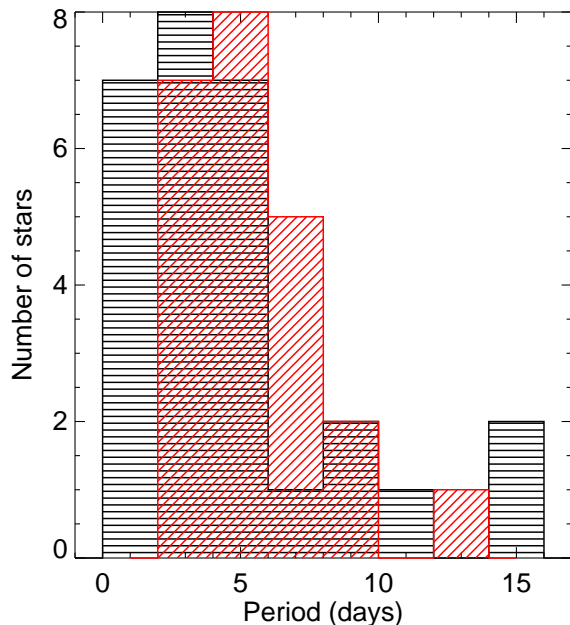


Fig. 4. Period distribution of CTTSs. The black histogram corresponds to spot-like LCs and the red histogram to the AA Tau-like LCs.

5. Conclusions

We showed that the AA Tau photometric behavior is common among CTTSs, being present in $28\% \pm 6\%$ of the CTTSs in our sample. This represents a lower limit, since the AA Tau-like LCs are more likely produced at high inclinations, and we are probably missing about 20% to 30% of the very high inclination systems, according to the calculations by Bertout (2000), which will be totally obscured by a flared disk and thus too faint to be observed by Corot.

If our interpretation of such systems is correct, the photometric minima are due to obscuring material located in the inner disk region, near the corotation radius. This material is built up through the interaction between an inclined stellar magnetosphere and the inner disk region. The observed periodical changes in width and depth of the observed minima, over a timescale of a few (~ 1 -3) rotational periods, would then reflect the dynamics of such an interaction, as predicted by MHD models of young low mass star-disk systems.

We compared the Corot light curves with *Spitzer* IRAC data of the same systems and showed that the agreement between classifications based on the two datasets is excellent. The percentage of AA Tau-like light curves, which are due to obscuration by circumstellar material in the inner disk region, varies as the inner disk dissipates, decreasing from $40\% \pm 10\%$ in systems

with thick inner disks to $36\% \pm 16\%$ in systems with anemic disks and none in naked photosphere systems. Indeed, $91\% \pm 29\%$ of the systems with naked photospheres exhibit pure spot-like variability, while only $18\% \pm 7\%$ of the thick disk systems do so, presumably those seen at low inclination and thus free of variable obscuration.

Acknowledgements. We thank Gabor Fűrész for making his Hectoechelle spectra and the updated electronic version of his tables available to us. We thank Cassandra Fallscheer for making available to us her table of U-V excess measurements. This research is based on data collected on the Corot satellite. SHPA and MMG acknowledge support from CNPq, CAPES and Fapemig. JFG acknowledges support from the FCT project PTDC/CTE-AST/66181/2006.

References

- Bertout, C., Basri, G., & Bouvier, J. 1988, *ApJ*, 330, 350
 Bertout, C. 2000, *A&A*, 363, 984
 Bouvier, J., Covino, E., Kovo, O., Martin, E. L., Matthews, J. M., Terranegra, L., & Beck, S. C. 1995, *A&A*, 299, 89
 Bouvier, J., et al. 2003, *A&A*, 409, 169
 Bouvier, J., et al. 2007, *A&A*, 463, 1017
 Carr, J. S. 2007, *IAU Symposium*, 243, 135
 Cieza, L., & Baliber, N. 2007, *ApJ*, 671, 605
 Dahm, S. E., & Simon, T. 2005, *AJ*, 129, 829
 Dahm, S. E. 2008, *Handbook of Star Forming Regions, Volume I: The Northern Sky* ASP Monograph Publications, Vol. 4. Edited by Bo Reipurth, p.966, 966
 DeWarf, L. E., Sepinsky, J. F., Guinan, E. F., Ribas, I., & Nadalín, I. 2003, *ApJ*, 590, 357
 Duchêne, G., et al. 2010, *ApJ*, 712, 112
 Fallscheer, C., & Herbst, W. 2006, *ApJ*, 647, L155
 Flaccomio, E., Micela, G., & Sciortino, S. 2006, *A&A*, 455, 903
 Fűrész, G., et al. 2006, *ApJ*, 648, 1090
 Goodson, A. P., Böhm, K.-H., & Winglee, R. M. 1999, *ApJ*, 524, 142
 Gustafsson, B., Edvardsson, B., Eriksson, K., Jørgensen, U. G., Nordlund, Å., Plez, B. 2008, *A&A*, 486, 951
 Hartmann, L., Hewett, R., & Calvet, N. 1994, *ApJ*, 426, 669
 Horne, J.H., & Baliunas, S.L. 1986, *ApJ*, 302, 757
 Kochukhov, O., 2007, *Physics of Magnetic Stars*, Proceedings of the International Conference, Editors: I. I. Romanyuk and D. O. Kudryavtsev, p.109-118
 Kulkarni, A. K., & Romanova, M. M. 2009, *MNRAS*, 398, 701
 Kupka F., Piskunov N.E., Ryabchikova T.A., Stempels H.C., Weiss W.W. 1999, *A&AS*, 138, 119-133
 Kupka F., Ryabchikova T.A., Piskunov N.E., Stempels H.C., Weiss W.W. 2000, *Baltic Astronomy*, vol. 9, 590-594
 Kurosawa, R., Harries, T. J., & Symington, N. H. 2006, *MNRAS*, 370, 580
 Lada, C. J., et al. 2006, *AJ*, 131, 1574
 Lamm, M. H., Bailer-Jones, C. A. L., Mundt, R., Herbst, W., & Scholz, A. 2004, *A&A*, 417, 557
 Matt, S., Goodson, A. P., Winglee, R. M., Böhm, K.-H. 2002, *ApJ*, 574, 232
 Ménard, F., & Bertout, C. 1999, *NATO ASIC Proc. 540: The Origin of Stars and Planetary Systems*, 341
 Muzerolle J., Hartmann L., & Calvet N. 1998, *AJ*, 116, 455
 Muzerolle J., Hartmann L., & Calvet N. 2001, *ApJ*, 550, 944
 Ramírez, S. V., et al. 2004, *AJ*, 127, 2659
 Rebull, L. M., Hillenbrand, L. A., Strom, S. E., Duncan, D. K., Patten, B. M., Pavlovsky, C. M., Makidon, R., & Adams, M. T. 2000, *AJ*, 119, 3026
 Rebull, L. M., et al. 2002, *AJ*, 123, 1528
 Rebull, L. M., Stauffer, J. R., Megeath, S. T., Hora, J. L., & Hartmann, L. 2006, *ApJ*, 646, 297
 Romanova, M. M., Ustyugova, G. V., Koldoba, A. V., & Lovelace, R. V. E. 2009, *arXiv:0907.3394*
 Rucinski, S. M., et al. 2008, *MNRAS*, 391, 1913
 Samadi, R., Fialho, F., Costa, J. E. S., Drummond, R., Pinheiro Da Silva, L., Baudin, F., Boumier, P., & Jorda, L. 2007, *arXiv:astro-ph/0703354*
 Scargle, J.D. 1982, *ApJ*, 263, 835
 Shu F., Najita J., Ostriker E., et al. 1994, *ApJ*, 429, 781
 Teixeira, P. S. 2008, Ph.D. Thesis
 White, R. J., & Basri, G. 2003, *ApJ*, 582, 1109
 Zanni, C. 2009, *Lecture Notes in Physics*, Berlin Springer Verlag, 791, 155

Table 1. Classical T Tauri stars that belong to NGC 2264 and were observed by Corot. The H α equivalent widths come from Rebull et al. (2002) and Dahm & Simon (2005), except for six stars (CID 223957455, 223959618, 223964667, 223968688, 223991832, 223994721) for which we measured the H α equivalent width ourselves, using the high resolution hectoechelle spectra kindly provided by Gabor Fűrész. The $U - V$ excesses were taken from Rebull et al. (2002) (UV1) and Fallscheer & Herbst (2006) (UV2, the U-V excess data table was provided by Cassandra Fallscheer). Stars that present H α width at 10% intensity larger than 270 km s $^{-1}$ are identified by a x sign in column eight, following the classification of Fűrész et al. (2006). The LC group and period values were determined in the present work. The α_{IRAC} index is described in Sect. 3.3 and comes from Teixeira (2008).

RA (deg)	Dec (deg)	V (mag)	Corot ID	H α EW (Å)	UV1 (mag)	UV2 (mag)	H α 10%	SpT	LC group	Period (days)	α_{IRAC}
99.89338	9.91424	16.64	223957455	22.1	x	...	NP
99.92281	9.77214	14.64	223959618	28.4	x	...	PII	3.87	...
99.99684	9.45681	16.34	223964667	42.2	x	...	PII	6.45	-1.87
100.04666	9.63501	16.67	223968039	52.9	-1.15	...	x	K6	NP	...	-1.35
100.05673	9.41375	13.02	223968688	0.60	x	K0	PI	1.11	-2.81
100.05710	9.94183	17.02	400007614	130.2	x	M2	NP	...	0.0149
100.09620	9.46176	16.04	223971231	49.5	-1.62	...	x	K5	NP	...	-1.73
100.09889	9.92330	17.55	223971383	80.6	x	...	PI	4.66	-1.22
100.12006	9.51718	15.20	223972652	39.1	-0.89	K4	NP	...	-0.56
100.12186	9.73542	17.69	400007809	31.3	-1.36	...	x	M2	NP
100.12859	9.57794	16.03	223973200	22.2	x	K1	NP	...	-1.29
100.13013	9.51864	15.43	223973292	1.7	-0.91	K6	PI	1.96	...
100.15217	9.84601	16.67	400007538	21.1	-2.11	-1.687	...	M2	NP	...	-1.29
100.15262	9.80638	15.62	500007298	4.9	-1.43	-0.606	...	K5	PI	15.70	-4.19
100.15781	9.58167	16.64	400007528	23.4	x	M3	NP	...	-1.87
100.16297	9.84961	15.43	500007252	46.5	-1.89	...	x	K4	PII	7.06	-1.55
100.16840	9.84735	15.50	500007272	58.3	K7	PI	3.76	-2.42
100.17086	9.46509	16.53	500007505	13.2	NP	...	-1.97
100.17095	9.79936	16.01	500007379	7.5	-1.22	-0.984	...	K7	PI	14.15	-1.97
100.17216	9.85066	15.70	500007315	24.5	-2.13	K7	PII	7.80	-1.19
100.17233	9.90385	13.57	223975844	12.2	0.02	...	x	G3	PI	3.31	...
100.17435	9.86237	15.49	500007269	23.4	K5	PI	3.75	-1.53
100.17576	9.56040	12.09	223976028	7.3	x	G0	NP	...	-1.12
100.18006	9.78535	16.33	500007460	27.1	x	K6	NP
100.18580	9.54061	18.13	500007930	60.0	M3	NP	...	-2.61
100.18819	9.47901	14.55	223976747	7.2	-0.16	...	x	K2	PII	3.16	...
100.19793	9.82471	14.14	500007120	12.8	...	-0.806	x	K1	PII	4.23	-1.41
100.19968	9.55087	18.24	500007963	-0.917	PI	2.56	...
100.20505	9.96077	17.46	500007730	50.8	M1	PI	11.85	-2.67
100.20789	9.61375	15.37	223977953	66.3	-1.79	-1.906	...	K4	PII	4.96	-1.43
100.21081	9.91593	15.13	500007209	11.2	x	K2	PII	2.51	-2.14
100.21326	9.74615	12.05	223978308	3.5	x	G0	PII	5.40	-1.69
100.22346	9.55686	14.70	223978921	18.2	...	-0.643	x	K1	NP	...	-2.29
100.22607	9.82232	16.39	500007473	161.1	-2.11	...	x	M0	NP	...	-0.38
100.22990	9.84718	15.89	500007354	2.8	-0.64	-0.774	...	K5.5	PI	1.17	-9.15
100.23215	9.85385	15.54	500007283	8.00	K5.5	PI	3.23	-0.29
100.23663	9.63029	15.09	223979728	113.2	...	-1.353	x	M1	NP	...	-1.17
100.24208	9.61483	18.05	223980048	34.0	PII	4.06	-1.41
100.24447	9.60368	17.40	223980233	22.2	M4	NP
100.24510	9.65522	17.02	223980258	27.9	x	M0	PI	7.05	-1.39
100.24516	9.51592	14.04	223980264	14.3	x	K2.5	PII	3.46	-1.51
100.24770	9.99596	15.34	223980412	7.41	-0.53	K5	PI	3.23	...
100.24792	9.49770	17.00	500007610	26.2	M3	PII	4.66	-1.16
100.24811	9.58636	15.58	223980447	6.4	-1.01	-0.427	x	K6	PI	1.67	-1.14
100.25209	9.75088	15.39	223980688	15.0	-0.59	-0.723	x	K3	PII	4.16	-2.10
100.25214	9.48776	14.56	223980693	16.6	x	K4	PII	5.35	-1.72
100.25323	9.85620	14.63	500007157	1.6	...	-0.658	...	K1	PI	4.36	...
100.25408	9.54568	13.51	223980807	6.4	x	K1	NP	...	-1.56
100.25767	9.64475	14.70	223981023	1.5	x	K4	PII	7.05	-2.41

Table 1. continued.

RA (deg)	Dec (deg)	V (mag)	Corot ID	H α EW (Å)	UV1 (mag)	UV2 (mag)	H α 10%	SpT	LC group	Period (days)	α_{IRAC}
100.26266	9.62660	19.17	500008211	34.1	M1	NP	...	-1.22
100.26503	9.50806	17.67	400007803	20.4	PII	9.75	-1.12
100.26789	9.41449	15.79	500007335	101.8	-2.34	...	x	M0	PII	7.36	-0.97
100.26905	9.64190	17.88	500007857	108.	M3	NP	...	-0.78
100.27071	9.84613	14.36	223981811	36.5	-0.29	-0.816	x	K1	PII	3.73	-1.91
100.27124	9.86239	15.39	500007248	1.7	-0.75	-0.570	...	K5	PI	1.88	-3.06
100.27583	9.60638	13.52	223982136	10.0	x	G3	PI	3.01	-2.03
100.27595	9.41769	18.01	500007896	34.7	M5	PI	9.30	-1.58
100.27679	9.47745	17.30	400007686	56.1	x	M1.5	NP	...	-1.57
100.27808	9.57943	15.97	500007369	49.4	x	G6	NP
100.28734	9.56278	17.53	500007752	51.0	x	M3	PI	4.01	-0.88
100.29582	9.59881	17.44	500007727	61.5	...	-2.037	x	K7	NP	...	-0.93
100.30241	9.87533	14.07	500007115	35.3	x	G	PII	2.01	-1.72
100.30362	9.43746	13.76	500007089	85.6	x	K4	NP	...	-1.33
100.31035	9.62065	17.23	500007667	4.1	...	-0.697	PI	5.41	-2.96
100.32188	9.90899	15.64	223985009	58.3	-2.40	K7	NP
100.32467	9.48364	18.55	500008049	231.4	M2.5	NP	...	-0.68
100.32534	9.64038	18.58	500008061	32.5	M3	PI	0.98	-2.89
100.32613	9.56488	15.02	223985261	28.9	-0.97	...	x	K4	NP	...	-2.39
100.33752	9.56005	15.20	223985987	10.6	x	K6	PII	3.31	-1.44
100.34851	9.78788	17.93	500007872	5.2	...	-0.767	PI	8.20	-2.01
100.35227	9.62653	17.38	400007709	8.9	-0.99	M3	PI	0.76	...
100.35677	9.57861	16.15	223987178	15.9	-0.61	-1.233	...	M0	PII	4.96	-1.11
100.36250	9.50365	17.47	400007734	25.8	M1	NP	...	-1.88
100.37968	9.44951	14.19	500007122	25.9	x	...	PII	12.53	-1.44
100.38169	9.80912	14.63	223988742	5.16	-0.08	-0.409	...	K2	PI	5.03	-2.84
100.38331	10.0068	15.59	223988827	13.1	K5	PI	4.78	-2.69
100.38543	9.63540	14.66	223988965	1.3	-0.67	K6	PI	3.23	-2.83
100.39397	9.60904	17.16	223989567	4.5	-0.83	...	x	M1	NP
100.40536	9.75186	15.44	223990299	35.0	...	-0.826	x	K4	PI	4.51	-0.93
100.41155	9.53661	15.40	500007249	58.6	x	K4	NP	...	-1.55
100.41564	9.67443	13.86	223990964	52.5	...	-1.061	...	K4	NP	...	-1.46
100.42867	9.41900	16.65	223991832	75.8	x	...	PII	8.40	-1.38
100.47104	9.96747	14.99	223994721	9.5	x	K7	NP	...	-1.47